Gain analysis of higher-order-mode amplification in a dielectric-implanted multi-beam traveling wave structure

Anthony Gee[1] and Young-Min Shin[1,2,a)]
[1]*Department of Physics, Northern Illinois University, Dekalb, Illinois 60115, USA*
[2]*Accelerator Physics Center (APC), Fermi National Accelerator Laboratory (FNAL), Batavia, Illinois 60510, USA*

A multi-beam traveling wave amplifier designed with an overmoded staggered double grating array was examined by small signal analysis combined with simulation. Eigenmode and S-parameter analyses show that the 2 cm long slow wave structure (SWS) has 1–5 dB insertion loss over the passband (TM_{31} mode) with ~28% cold bandwidth. Analytic gain calculation indicates that in the SWS, TM_{31}-mode is amplified with 15–20 dB/beam at 64–84 GHz with three elliptical beams of 10 kV and 150 mA/beam, which was compared with particle-in-cell (PIC) simulations. PIC analysis on the analysis of instability with zero-input driving excitations demonstrated that background noises and non-operating lower order modes are noticeably suppressed by implanting equidistant dielectric absorbers; the overmoded structure only allowed the desired 3rd order mode to propagate in the structure. The designed circuit structure can be widely applied to multi-beam devices for high power RF generation.

I. INTRODUCTION

Microwave power modules (MPMs)[1,2] have revolutionized microwave transmitter systems by combining the best of solid-state and vacuum electron device technologies to achieve dramatic increases in the W/cm^3 and W/g, which are critical figures for space and prime power limited systems such as those employed in airborne and space-borne platforms. MPMs with power exceeding 250 W have been demonstrated in the 3–18 GHz band[3] and traveling wave tube (TWT) designs have been demonstrated with >100 W output power in the 18–35 GHz band for possible use in MPMs.[4] Typically, MPMs can achieve overall efficiency >35% for broadband and >50% for narrow band applications.[5] The accomplishments of MPM technology in microwave bands have been very impressive with power exceeding 100 W at frequencies in the Ka-band and lower. However, several recent developments in communication systems have fueled the development of communication systems at higher frequencies. This requirement has been largely driven by the need for transmitting and receiving extensive amounts of data for real time remote navigation and target identification necessary in the new paradigm in military warfare, the Unmanned Aerial Vehicle (UAV). The current data requirements necessitate operation at V-band (50–75 GHz) and in the near future at W-band (75–110 GHz) to transmit real time video via a satellite link. However, MPMs with >50 W output have not yet been demonstrated above Ka band, which has not translated into similar performance in the millimeter wave band (>30 GHz). The development of a higher power, higher gain TWT is the most critical requirement for the eventual development of a millimeter wave MPM. Overmoded interaction circuits at millimeter and sub-millimeter waves have the potential for generating higher power by (a) increasing the total beam current flowing through the circuit and (b) by reducing the ohmic loss in the circuit. However, operation in overmoded circuits is challenging for two reasons. First, when compared to fundamental mode circuits they have lower interaction impedance, which is a measure of the beam-wave coupling. Second, the overmoded circuits support lower order modes at frequencies below the operating mode, which have a stronger coupling to the electron beam than higher order modes. This causes mode competition which limits stable single mode in-band operation, which is essential for a power amplifier in a communication system.

The diminished interaction impedance in an overmoded circuit can be offset or even exceeded by the use of multiple electron beams coincident with the multiple maxima of the higher order mode. This provides the unique advantage of lowering a voltage ($=V_0/n_b$) by increasing total beam current ($=n_b \times I_0$) with the same total beam power ($=I_0V_0$), where n_b is the number of beams. This will result in a higher value of the Pierce gain parameter/beam, C ($=(n_b^2K_mI_0/4V_0)^{1/3}$), where K_m is the interaction impedance/beam,[6] I_0 is the beam current/beam, and V_0 is the voltage (Here, the Pierce parameters are calculated with only a single beam as each beam independently interacts with a higher order mode at its maximum field positions.) On the other hand, if a given total beam current (I_0) is split into n_b beams ($I_b = I_0/n_b$), the magnetic field ($\sim I_0^{1/2}/V_0^{1/4}$) required for beam focusing can be lowered proportional to $n_b^{1/2}$ at the same beam voltage ($V_b = V_0$), which may though slightly drop gain/beam with $n_b^{1/3}$. Lowering the magnetic focusing field is critical for space and weight limited systems such as MPMs. However, the multi-beam operation leaves the problem of mode competition from the lower order modes, which is the main inhibitor in the adoption of such overmoded slow wave structure (SWS) circuits. It is well known[7,8] that higher-order-mode (HOM) structures with dielectric-absorbers or -filters suppress the lower order modes, while not affecting the operating HOM. Also, unwanted neighboring parasitic modes or the oscillations at the cutoff

a)yshin@niu.edu

Operated by Fermi Research Alliance, LLC under Contract No. De-AC02-07CH11359 with the United States Department of Energy.

frequencies of passbands can be suppressed with lossy dielectric buttons.[6]

To explore a feasible way of generating high power at millimeter wave, we extended the concept of the overmoded structure with a dielectric-implanted staggered double grating array (SDGA).[9] Recently, the SDGA type SWS has been widely studied for intense RF generation at millimeter and sub-millimeter wave bands as they provide broad spectral coverage and high radiation efficiency. In this paper, the circuit was designed for >100 W of output power across V-band with >30% bandwidth: 73.5 GHz center frequency and ~5 GHz operating bandwidth (71–76 GHz). For practical drive amplifier performance, we constrain the input driving power to 100 mW. This paper will discuss Pierce gain analysis, which is combined with electromagnetic (EM) simulations, and particle-in-cell (PIC) simulations of the 3-beam overmoded structure with 50 mA/beam and 150 mA/beam, including system stability analysis performed for a long simulation time.

II. SWS DESIGN

The interaction structure is a dielectric loaded staggered double grating waveguide as shown in Fig. 1(a). The half-period staggering of a pair of 1-D vane arrays[10,11] results in a strong, symmetric axial electric field distribution of the fundamental mode along the direction of the electron beam propagation. The transverse field distribution of the first three modes of the structure is shown in Fig. 1(b). The circuit operates in the forward fundamental mode and to achieve low voltage (10 kV) operation we choose to operate the circuit at the second forward space harmonic ($n = 1$) corresponding to 2π–3π range of phase advance per cell.

The unique properties of the double staggered grating waveguide offer high gain and wide bandwidth.[12–17] An added advantage of the structure is its inherent compatibility with a multiple-beam configuration to achieve higher output power.[18,19] The in-circuit combination of gain and output power offered by multiple beams in an overmoded circuit eliminates the need for complicated and lossy external power combining schemes such as those involving quasi-optical techniques. The total output power is expected to be a sum of the power extracted from each beam and, so ideally kilowatt level power could be achieved by increasing the number of beams.

We have optimized the dimensional parameters to achieve a broad cold bandwidth of ~20 GHz (~28%): period $d = 1$ mm, beam tunnel height $b = 0.45$ mm, waveguide width $3h = 7.56$ mm, vane height $L = 1$ mm, vane thickness $s = 0.25$ mm, cavity length $a = 0.75$ mm. For the simple simulation analysis, a slow wave structure is first designed with four dielectric plates (top and bottom) for TM_{31}–mode, as shown in Figure 1(a), which are composed of aluminum nitride (AlN) with $\varepsilon_r = 8.6$ and $\tan\delta = 0.0003$ and the electrical conductivity of the waveguide is $\sigma = 5.8 \times 10^7$ S/m corresponding to that of oxygen-free high conductivity copper. Figure 1(c) shows the dispersion curves of the first three modes (TM_{11}, TM_{21}, TM_{31}). Our optimized dimensions give a mid-band frequency of 73.5 GHz corresponding to the TM_{31} mode. In Fig. 1(c), our 10 kV beam line lies along the forward phase of the TM_{31} mode, indicating highest coupling between our TM_{31} mode and the electron beam. The dielectric loading also imposes heavy losses on the parasitic modes (TM_{11}, TM_{21}) and reduces their ohmic Q (Q_0).

Figure 2 shows transmission characteristics for a 2 cm long circuit (20 cells) with and without dielectric loading. Without the absorbers, transmission losses for all modes are approximately the same, 1–5 dB, corresponding to 0.5–2.5 dB/cm attenuation. By implanting four lossy AlN plates, TM_{31} shows

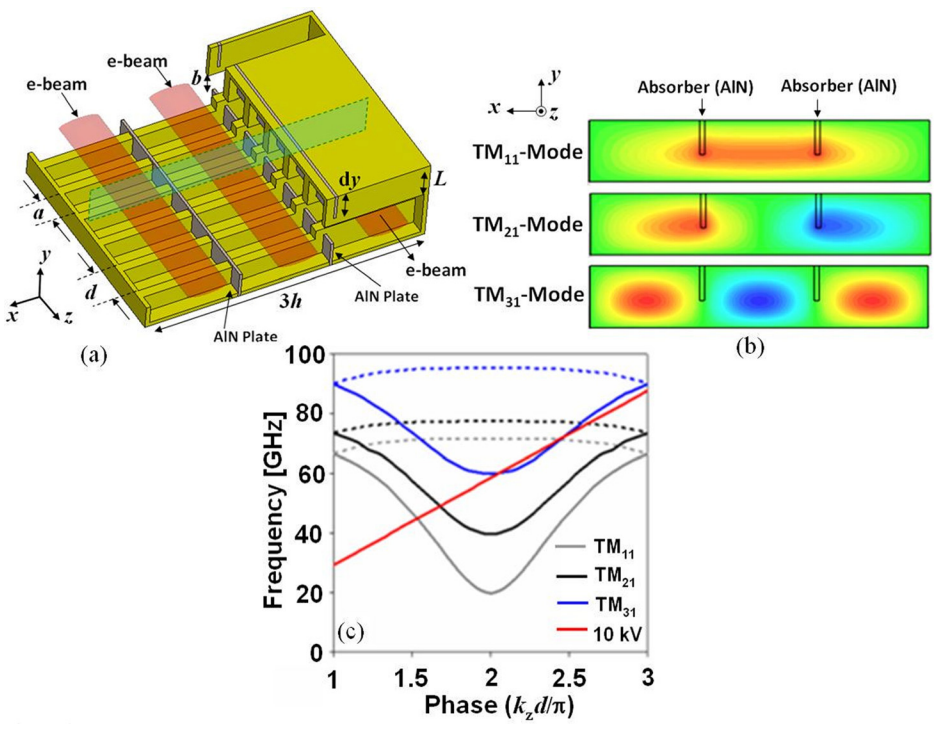

FIG. 1. (a) Dielectric loaded multi-beam traveling wave amplifier with AlN absorbers (top and bottom), (b) electric field (E_z) distribution of the first three modes of the circuit at the plane denoted in Fig. 1(a) (the green-colored box in the dashed line of Fig. 1(a) is the area for the field plots of Fig. 1(b)), (c) dispersion curves of three slow wave modes (TM_{11}, TM_{21}, and TM_{31}) and 10 kV beam line.

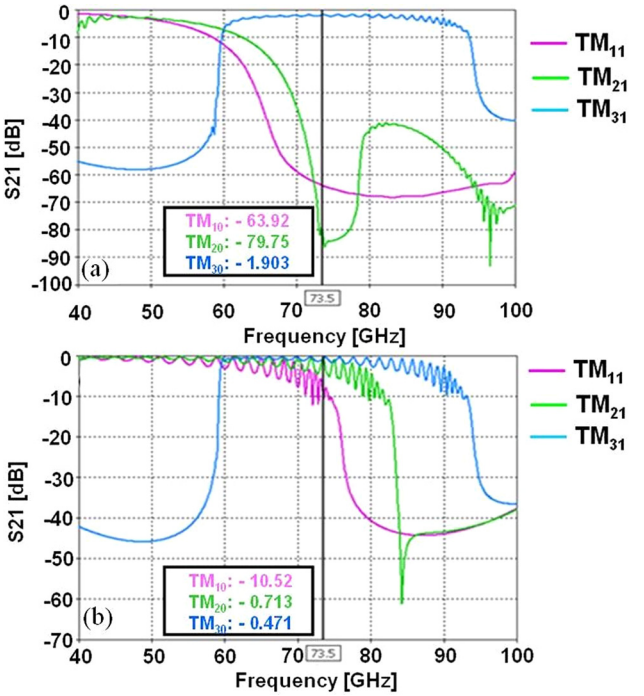

FIG. 2. Transmission of the TM_{11}, TM_{21}, and TM_{31} modes in an overmoded double grating waveguide (a) without and (b) with implanting AlN absorbers.

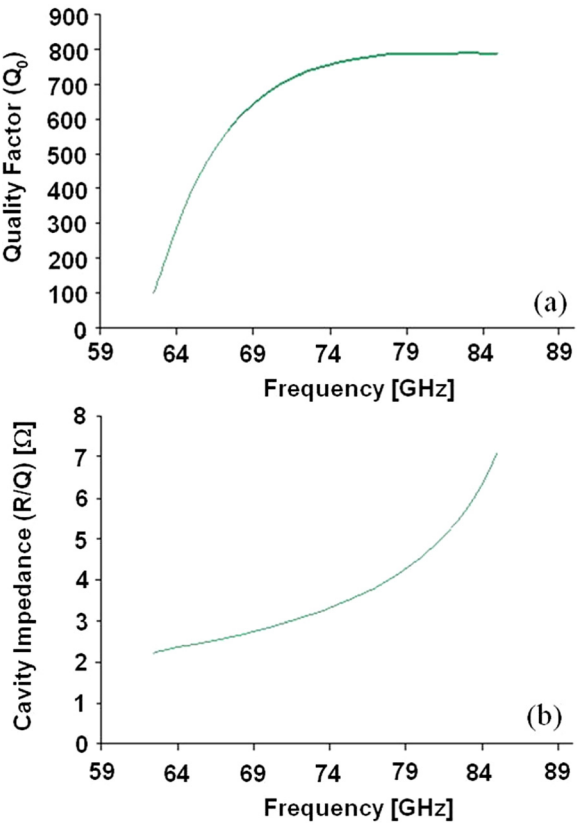

FIG. 3. (a) Quality factor (Q_0) and (b) cavity impedance (R/Q) versus frequency of the unit cell for $L = 1$ mm.

to have the nearly same transmission spectrum with minimal loss, while the parasitic modes are immediately suppressed down to <50 dB, which therefore leads to selection of TM_{31} mode as the operating mode. It is sufficient that the parasitic modes are suppressed in the operating band.

III. THEORETICAL ANALYSIS

For theoretical assessment to predict gain of three beam power amplification,[6,20] we calculated quality factor (Q_0) and circuit impedance (R/Q) per unit cell ($R/Q = ((\int_{-\infty}^{\infty} |E_z|dz)^2/2\omega W)$) from the FIT (Finite-Integration-Technique) based eigenmode simulations,[21] where W is stored energy in the cavity volume. Figure 3 shows the quality factor (Q_0) and cavity impedance (R/Q) versus frequency for the unit cell in a circuit with a vane height of $L = 1$ mm circuit. As shown in the figure, the quality factor is quite high, ~770, and stable around the operating frequency. The theoretical Pierce interaction impedance is calculated using the built-in computational post-processor in the numerical solver. The interaction impedance (K_m) is given by

$$K_m = \frac{|E_m|^2}{2\beta_m^2 P}, \tag{1}$$

where

$$E_m = \frac{1}{d}\int_0^d E_z(z)e^{j\beta_m z}dz \tag{2}$$

and P ($=\omega W/Q_0$) is the power flow, where $W = 1$ J, which is the default input energy in the EM simulation, and $\beta_m = (\varphi_0 + 2m\pi)/d$ is the propagation constant of the mth space harmonic, where d is the periodic length. The electric field data (E_z) are directly obtained from 3D-EM simulation, which is programmed with a periodic boundary between the master and slave planes in a unit cell. The interaction impedance for the $L = 1$ mm circuit is shown in Fig 4(a). It is typical for K_m to be high at the lower cutoff, but the beam-wave coupling is minimal due to lack of synchronization, as shown in the dispersion relation in Fig. 1(c).

The Pierce gain parameter (C) is calculated using K_m by the formula,

$$C = \left(\frac{K_m I_b}{4V_b}\right)^{1/3} \tag{3}$$

where I_b and V_b are the beam current and voltage, respectively. The TM waves propagate in the form of $A_n exp(j\omega t - \Gamma_{nz})$, where $n = 1$, 2, and 3 is the wave index and Γ is the complex propagation constant. For the forward wave of our interest, Γ is defined as

$$\Gamma = j\beta_e - \beta_e C\delta, \tag{4}$$

where δ is the incremental propagation constant and β_e is the beam wave vector. One can see that the incremental propagation constants determine the fundamental circuit parameters and most importantly the total gain achieved by the circuit. The determinantal equation, whose roots determine δ, is given by

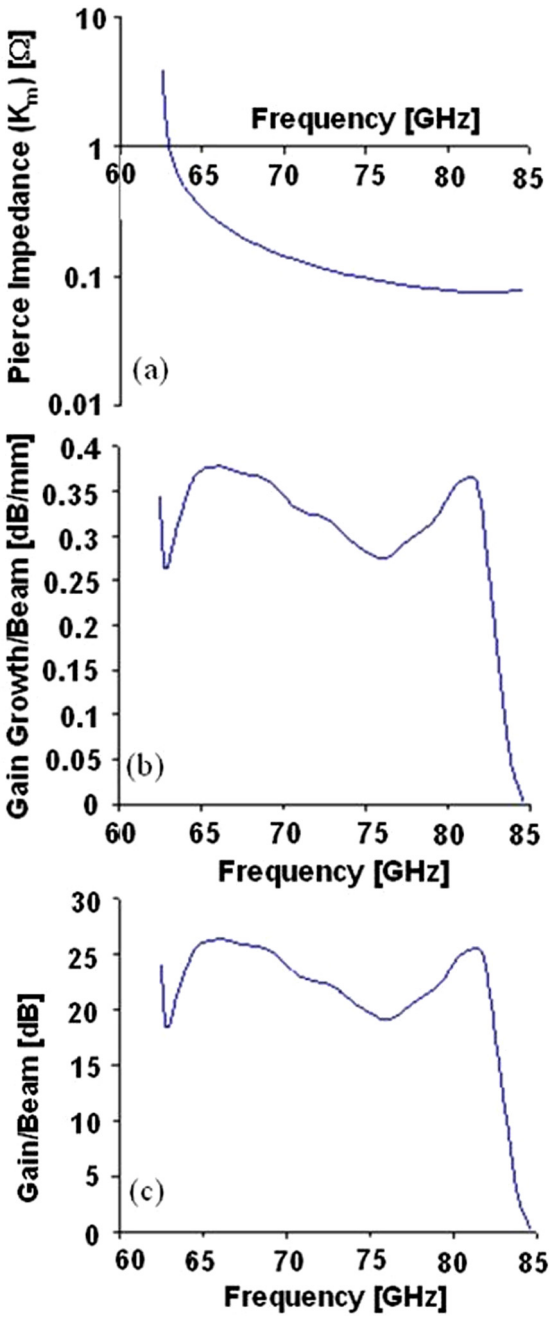

FIG. 4. (a) Pierce impedance (K_m), (b) gain growth/beam, (c) gain/beam vs. frequency of the unit cell for $L = 1$ mm

$$\delta^2 = \left[\frac{1}{-b + j(d_0 + \delta)}\right] - 4QC, \tag{5}$$

where b is the Pierce velocity parameter,

$$b = \frac{1}{C}\left(\frac{\beta_m}{\beta_e} - 1\right), \tag{6}$$

d_0 is related to the circuit loss (L_0) in dB/wavelength,

$$d_0 = \frac{L_0}{20(\log e)2\pi C} \tag{7}$$

and $4QC$ is the Pierce space charge

$$4QC = \frac{\beta_q^2}{\beta_e^2 C^2}, \tag{8}$$

where β_q is the reduced plasma propagation constant. Equation (5) is cubic in δ and has three roots representing the forward and backward waves. Of the three forward waves, in general only an increasing wave with velocity less than the electron beam may be amplified. With a sufficiently long circuit, only the amplified wave contributes to the gain.

The launching loss, η_i, is determined by the δ's and modulated by the space charge and is given by[6]

$$\eta_i = \frac{1 + \frac{4QC}{\delta_i^2}}{\prod_{i=1}^{k}\left(1 - \frac{\delta_k}{\delta_i}\right)}. \tag{9}$$

Thus, the total gain in the circuit is given by

$$G = 10\log\left(\left|\sum_{i=1}^{3} \eta_i \exp(\Gamma_i l_c)\right|^2\right), \tag{10}$$

where l_c is the circuit length, and Γ_i is determined by Eq. (4). In summary, to calculate total gain, the essential parameters are the Pierce interaction impedance, K_m, and the incremental propagation constants, δ_i. Once calculated, total gain, as contributed by all three forward waves, may be determined. Another useful quantity is gain growth rate, which is simply G/l_c and is shown for the $L = 1$ mm circuit in Fig. 4(b). The full gain is shown in Fig. 4(c). The total gain for the $L = 1$ mm circuit with $l_c = 7$ cm (70 periods) is approximately 21 dB within the operating band of 71–76 GHz. Ideally, a circuit length $l_c = 10$ cm (100 periods) would provide 30 dB gain, corresponding to 100 W output power from 100 mW input power.

IV. PIC SIMULATION ASSESSMENT

The results are used to predict the circuit performance based on a unit cell of the structure, which includes the space charge effects, circuit loss and launching loss. We extensively analyze the designed SDGA structure with vane height of $L = 1$ mm and circuit length of $l_c = 7$ cm with a full 3D PIC simulation.[22] The structural dimensions are precisely described in Sec. II. In the model, the background material is defined with a perfect conductor at the transverse walls and an open boundary at the end of the drift tube. The model has three elliptical sheet electron beams. The beam voltage, V_b, is 10 kV and the beam current, I_b, is 50 mA/beam (simulation-I) and 150 mA/beam (simulation-II), resulting in 150 mA and 450 mA for total beam current respectively, which are focused with a 1 tesla solenoid field. The AlN plates are 0.87 mm high and 0.075 mm wide. The long AlN plates may possibly be fabricated by micromachining, laser ablation, or thermal plasma etching.[23–25] It was found that a circuit width $3h = 7.56$ mm shows maximum gain at the lower end of the cold bandwidth of the circuit in the PIC simulation. The model is simulated for 3 ns to avoid inclusion of any possible cutoff oscillation

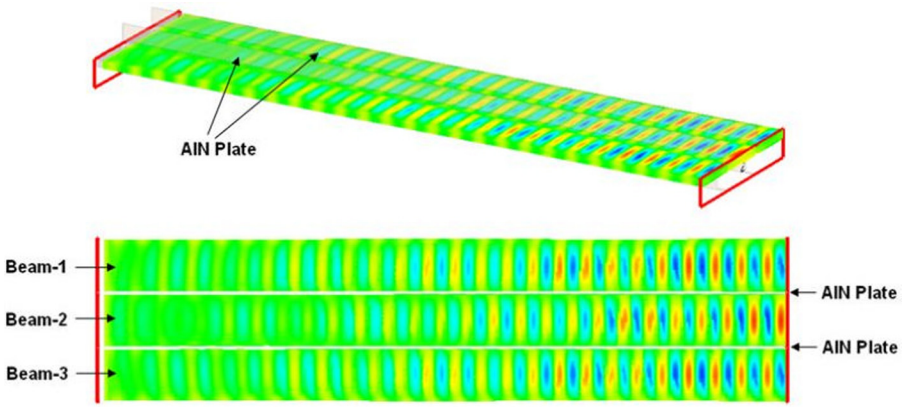

FIG. 5. PIC simulation result (electron energy distribution) of the designed circuit with $l_c = 7$ cm. The electron bunching in the 2nd beam is anti-phased (phase difference = 180°) with that of the 1st and 3rd beams.

and numerical noise excitation in the signal amplification as the signal reflections from the circuit terminals begins to destabilize the signal amplification. With the center of the transverse plane being the origin, the plates are placed at $(\pm h/2, \pm b/2, \pm L)$, ending with four plates placed at the maximum of the transverse fields for the parasitic modes. In Fig. 5, energy distribution of the full 3D PIC simulation shows that the three beams are mono-energetically modulated with a single frequency of TM_{31} mode as they have 180° phase-difference in the energy distributions. Note that the beam at the center has slower bunching transition than the other two as the field of the center is relatively weaker than those of the sides. Figure 6(a) shows the time-evolution of the gain at 71 GHz, calculated from the input (100 mW) and output powers monitored at the input and output ports. The gain converges to ~18 dB around 1.3 ns. One can see that TM_{31} mode is stably growing with only very small fluctuation. We swept driving frequencies from 68 GHz to 78 GHz with a 0.5 GHz step using the same PIC simulation model. For the parametric estimate, it was specified that the frequencies are all driven at 100 mW, the maximum power provided by a solid-state amplifier driver. Figure 6(b) shows the comparison between the theoretical gain and the simulated one. The comparison shows that the circuit gain is significantly below the ideal gain. It might be attributed to the fact that some frequency points of PIC simulations are excessively saturated with 100 mW, while the others are under-saturated with the input power. The designed input power of 100 mW could be significantly off the maximum saturation point in the operating band. To produce a saturated gain curve would require extensive examination of input powers at each frequency point. Besides, the initial theoretical calculation considered circuit loss to be negligible. Including moderate circuit loss, $d_0 = 1$, corresponding to ~0.278 dB/wavelength at mid-band, the theoretical gain becomes as shown in Figure 6(c). The PIC simulation model does not include an impedance matching or transition section at the two end circuit terminals. Any intrinsic noise signals from the mismatch could disturb normal signal amplification. Implementing the matching load with smooth transition or increase of the surface resistivity in the simulation model might thus possibly mitigate the discrepancy. More practically, a tapered vane coupler could provide a proper impedance matching with the overmoded staggered vane slow wave circuit.[26]

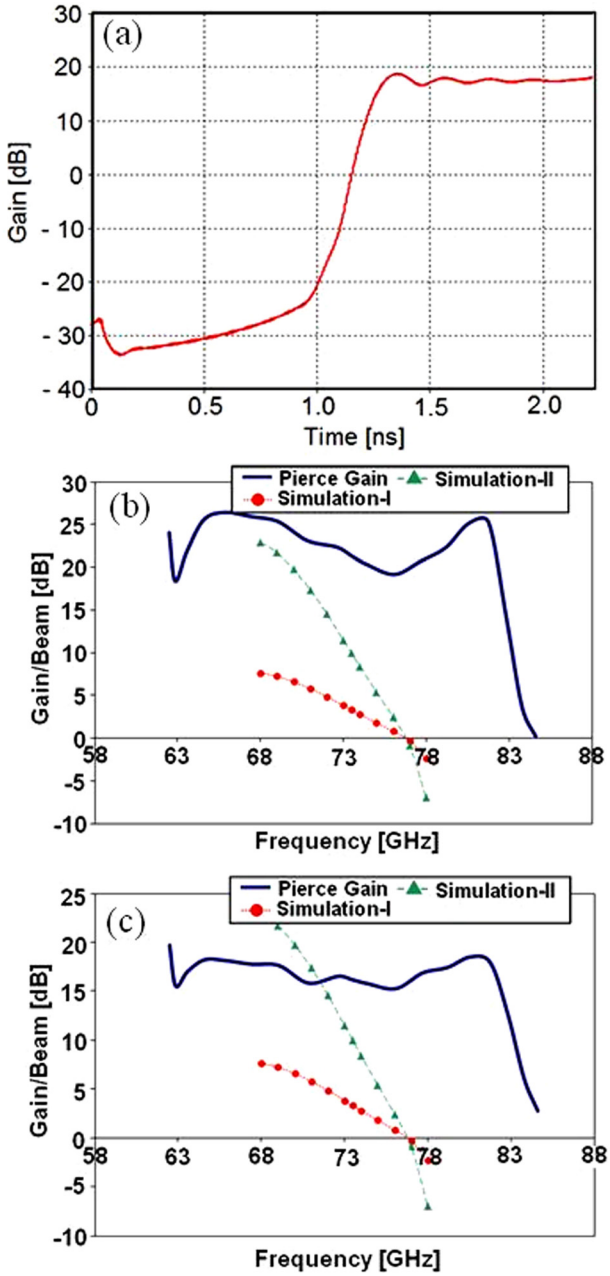

FIG. 6. (a) Gain versus time graph, calculated from PIC simulation at 71 GHz input driving frequency. Gain versus frequency graphs from theory and simulations (simulation-I: $I_b = 50$ mA, simulation-II: $I_b = 150$ mA) (b) without loss ($d_0 = 0$) and (c) with loss ($d_0 = 1$).

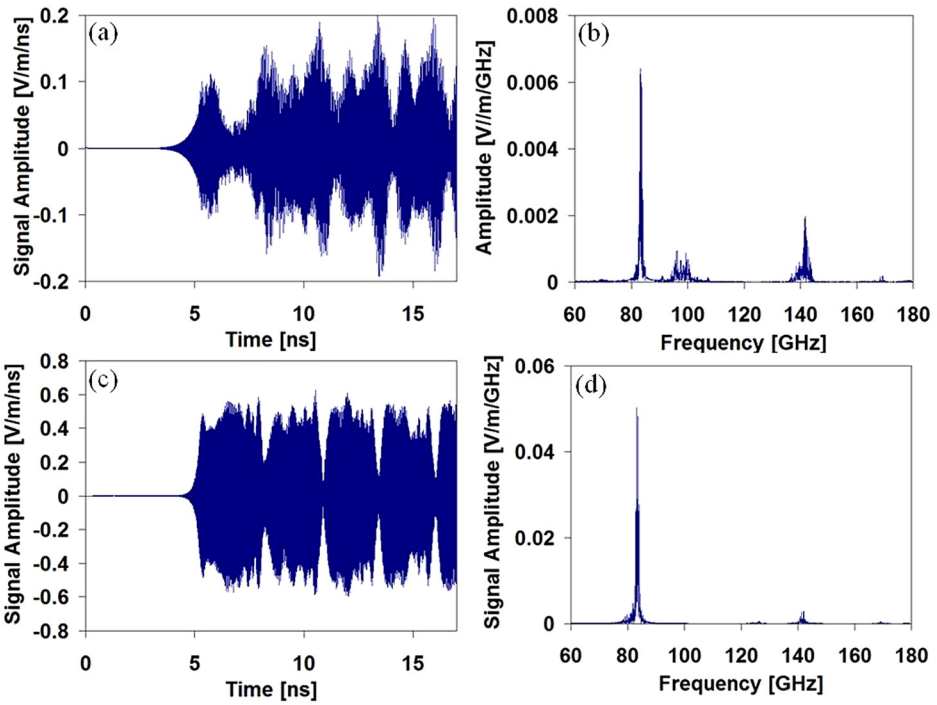

FIG. 7. (a) Input port signal with zero driving signal and (b) fast Fourier transformed (FFTed) input port spectrum (c) output port signal with no driving signal and (d) FFTed output port spectrum.

Finally, stability of the designed circuit was examined with no driving signal. For the stability investigation, the input and output signals of the circuit were analyzed with 10 kV and 150 mA/beam without input power. Comparing Figures 7(a), 7(b) and 7(c), 7(d), obtained from the long period simulation (~17 ns), one can see that the circuit has some degree of zero-driving noise excitation and signal amplification. However, the excited signals dominantly appear just after 5 ns and in the time interval (~3 ns) where the circuit was simulated in Figure 6(a), the spectra show no signal excitation. It implies that the instantaneously excited noise signals due to the abruptly loaded beam, as shown in Figures 7(a) and 7(b), could grow up due to intrinsic circuit reflections and return losses at the external ports. There is a possibility of reflection instability with a low loss structure typically with a small signal gain of ~40 dB. Assuming a net match of ~10 dB at the input and the output, then >20 dB of distributed loss (or sever) will need to be added to the circuit to ensure stability. Beyond the operating band, the spectrum also has a peak around 145 GHz resulting from a higher order mode excitation due to a beam-wave coupling, which will vanish with increasing the length of the structure as signal amplification does not occur due to de-synchronization of the high frequency component. Insertion of a sufficient return loss with a coupler or lossy circuit wall will sufficiently suppress any standing waves or signal reflections of the operating mode (TM_{31}) that will stabilize the circuit performance.[26]

V. CONCLUSION

The analytic estimate of gain characteristics of the overmoded multi-beam amplifier has been presented with numerical calculations. The analysis shows some degree of agreement with PIC simulations, which would still need to be improved though. The optimization of the design analysis and modeling process is currently underway. The analysis results have, nevertheless, promised the HOM SWS for multi-beam operation in offering a practical level of gain for high power generation. In the millimeter wave regime, our theoretical calculation predicted optimal performance of the designed circuit with ~21 dB over the passband of the TM_{31}-mode. PIC simulations show similar trends to the analytic gain calculations. Including moderate circuit loss, the simulated and theoretical gain is in closer agreement. A stability investigation was performed and showed the circuit likely has stable behavior in short burst operation. It will be necessary to introduce loss to attenuate the reflected and standing waves to prevent amplification. In addition to the structure described here, other structure designs to improve interaction impedance were examined and an in-depth analysis of these new designs will hold potential for higher efficiency in a narrower band. The presented analysis method will be used for design of overmoded HOM structures with rapid prediction of output performance of high power multi-beam devices.

ACKNOWLEDGMENTS

This work was funded as subcontract from Bridge 12 Technologies, Framingham, MA under a Small Business Innovation Research (SBIR) Phase I grant (Contract #: FA8650-12-M-1440) from the U.S. Air Force. This submission was approved for public release on 2013-06-06 (PA#: 88ABW-2013-2659).

[1]R. H. Abrams, Jr. and R. K. Parker, "Introduction to the MPM: what it is and where it might fit," Microwave Symp. Dig. **1**, 107–110 (1993).
[2]C. R. Smith, C. M. Armstrong, and J. Duthie, "The microwave power module: a versatile RF building block for high-power transmitters," Proc. IEEE **87**(5), 717–737 (1999).
[3]Tom Ninnis, "Microwave Power Modules; Miniature Microwave Amplifiers for UAVs," L-3 Communications Corporation. Electron Devices Division; http://www2.l-3com.com/edd/pdfs/uavpaper.pdf.

[4]A. Katz, R. Gray, and R. Dorval, "Performance of Microwave and Millimeter Wave Power Modules (MPMs) with Linearization," Linear Technology Inc.; http://www.lintech.com/PDF/L-MPM.pdf.
[5]R. J. Barker, N. C. Luhmann, J. H. Booske, and G. S. Nusinovich, *Modern Microwave and Millimeter-Wave Power Electronics* (Wiley-VCH, 2005), p. 872.
[6]J. F. Gittins, *Power Traveling Wave Tubes* (Electronics Research Laboratories, American Elsevier, New York, 1965).
[7]E. I. Smirnova, A. S. Kesar, I. Mastovsky, M. A. Shapiro, and R. J. Temkin, "Demonstration of a 17-GHz, high-gradient accelerator with a photonic-band-gap structure," Phys. Rev. Lett. **95**, 074801 (2005).
[8]E. N. Comfoltey *et al*., "Design of an overmoded W-band TWT," in *Vacuum Electronics Conference (IVEC'09)* (IEEE International, 2009), pp. 127–128.
[9]Y.-M. Shin, Phys. Plasmas **19**, 053102 (2012).
[10]Y.-M. Shin and L. R. Barnett, Appl. Phys. Lett. **92**, 091501 (2008).
[11]Y.-M. Shin, L. R. Barnett, and N. C. Luhmann, Jr., Appl. Phys. Lett. **93**, 221504 (2008).
[12]T. Ishibashi, N. Hayashizaki, T. Hattori, T. Ito, L. Lu, and J. Tamura, "Multi-beam cavity for low energy beam acceleration," Nucl. Instrum. Methods Phys. Res. B **261**, 13–16 (2007).
[13]E. J. Kowalski, M. A. Shapiro, and R. J. Temkin, "Over-moded W-band traveling wave tube design," in *IEEE Thirteenth International Vacuum Electronics Conference (IVEC)*, 2012.
[14]E. S. Lee *et al*., "Terahertz band gaps induced by metal grooves inside parallel-plate waveguides," Opt. Express **20**(6), 6116–6123 (2012).
[15]J.-K. So, H.-C. Jung, S.-H. Min, K.-H. Jang, S.-H. Bak, and G.-S. Park, "Enhanced transmission of electromagnetic waves through 1D plasmonic crystals", Opt. Express **18**(19), 20222 (2010).
[16]W. Liu, Z. Yang, Z. Liang, D. Li, K. Imasaki, Z. Shi, F. Lan, G.-S. Park, and S. Liu, "Enhancements of terahertz radiation from a grating waveguide by two-stream instability," IEEE Trans. Plasma Sci. **36**(3), 748–756 (2008).
[17]K.-H. Jang, S.-G. Jeon, J.-I. Kim, J.-H. Won, J.-K. So, S.-H. Bak, A. Srivastava, S.-S. Jung, and G.-S. Park, "High order mode oscillation in a terahertz photonic-band-gap multibeam reflex klystron," Appl. Phys. Lett. **93**, 211104 (2008).
[18]G. S. Nusinovich, S. J. Cooke, M. Botton, and B. Levush, "Wave coupling in sheet- and multiple-beam traveling-wave tubes," Phys. Plasmas **16**(6), 063102 (2009).
[19]H. P. Freund, D. Douglas, and P. G. O'Shea, "Multiple-beam free-electron lasers," Nucl. Instrum. Methods Phys. Res. A **507**, 373–377 (2003).
[20]J. R. Pierce, *Traveling-Wave Tubes* (Van Nostrand, New York, 1950).
[21]CST Microwave Studio Suite version 2012.
[22]CST Particle-Studio Suite version 2012.
[23]S. H. Kim, T. Balasubramani, I.-B. Sohn, Y.-C. Noh, J. Lee, J. B. Lee, and S. Jeong, "Precision microfabrication of AlN and Al_2O_3 ceramics by femtosecond laser ablation," Proc. SPIE **6879**, 687910 (2008).
[24]S. Saravanan, E. Berenschot, G. Krijnen, and M. Elwenspoek, "A novel surface micromachining process to fabricate AlN unimorph suspensions and its application for RF resonators," Sens. Actuators A **130–131**, 340–345 (2006).
[25]F. A. Khan, L. Zhou, V. Kumar, I. Adesida, and R. Okojie, "High rate etching of AlN using BCl3/Cl2/Ar inductively coupled plasma", Mater. Sci. Eng. B **95**, 51–54 (2002).
[26]Y.-M. Shin, L. R. Barnett, and N. C. Luhmann, Jr., "Phase-shifted traveling wave tube circuit for ultra-wideband high power submillimeter wave generation," IEEE Trans. Electron. Devices **56**(5), 706 (2009).